Available online at www.sciencedirect.com
SCIENCE DIRECT®
Applied Catalysis A: General 259 (2004) 83–94
APPLIED CATALYSIS A: GENERAL
www.elsevier.com/locate/apcata

CO formation/selectivity for steam reforming of methanol with a commercial $CuO/ZnO/Al_2O_3$ catalyst

H. Purnama [a], T. Ressler [a,*], R.E. Jentoft [a], H. Soerijanto [a], R. Schlögl [a], R. Schomäcker [b]

[a] *Department of Inorganic Chemistry, Fritz-Haber-Institut der Max-Planck-Gesellschaft, Faradayweg 4-6, Berlin D-14195, Germany*
[b] *Institut für Chemie, Technische Universität Berlin, Straße des 17. Juni 124, Berlin D-10623, Germany*

Received in revised form 11 August 2003; accepted 9 September 2003

Abstract

A study of CO formation for steam reforming of methanol on a commercial $CuO/ZnO/Al_2O_3$ catalyst has been performed in the temperature range 230–300 °C and at atmospheric pressure. The reaction schemes considered in this work are the methanol–steam reforming (SR) reaction and the reverse water gas-shift (rWGS) reaction. Power rate laws for the SR and reverse WGS reactions were used in a refinement of rate equations to the experiment data. For the temperature range studied the reaction order of methanol was determined under differential conversion (less than 10%) and was found to be 0.2. The integral method (partial pressure of the reactants and products measured as a function of contact time) was then applied to determine the reaction rate constants, activation energies, and pre-exponential factors for both reactions. The experimental results of CO partial pressure as a function of contact time at different reaction temperatures show very clearly that CO was formed as a consecutive product. The implications of the reaction scheme, in particular with respect to the production of CO as a secondary product, are discussed in the framework of on-board production of H_2 for fuel cell applications in automobiles. Potential chemical engineering solutions for minimizing CO production are outlined.

Keywords: Methanol–steam reforming; Commercial catalyst $CuO/ZnO/Al_2O_3$; Reaction kinetics; CO formation; Intraparticle diffusion limitation; Dilution effect; Reverse water gas-shift reaction

1. Introduction

Interest in hydrogen production for fuel cell powered automobiles is increasing for environmental reasons and for high energy efficiency. There are only a few fuel candidates that can be used in a reforming process to produce hydrogen on-board. Four of the best candidates are methanol, ethanol, gasoline, and diesel. The comparison of these fuels concerning their application for on-board reforming has been performed in the work of Lindström and Pettersson [1]. Methanol is found to be the most favorable candidate due to a low reaction temperature and the high ratio of hydrogen to carbon. One of the main drawbacks of methanol–steam reforming is the formation of CO as a by-product to the major products hydrogen and carbon dioxide. In the methanol–steam reforming process over copper-based catalysts, the amount of CO in the dry product stream at high methanol conversion is 10^3–10^4 ppm, at least 50 times more than the amount allowed in fuel cell applications (<20 ppm). A study of the deterioration in performance of a proton-exchange membrane fuel cell (PEMFC) due to impurities such as CO, CH_4, HCHO, and HCOOH in the hydrogen fuel has been recently reported [2]. By introducing 20 ppm CO to the fuel cell the current density decreased to about 18% within 210 h. In comparison to other impurities, the poisoning effect of CO was found to have the largest influence on the fuel cell performance.

Generally, there are three possibilities to prevent CO from being introduced into the fuel cell: (i) an extra module is added between the steam reforming reactor and the fuel cell (CO clean-up unit), such as separation of hydrogen using Pd membranes or the selective oxidation of CO [3–5], (ii) a new design for the reformer reactor is employed, i.e. purification integrated in the reformer reactor [6–10], or (iii) a new catalyst is developed that is active for steam reforming, but does not produce CO.

* Corresponding author. Tel.: +49-30-8413-3192; fax: +49-30-8413-4401.
E-mail address: ressler@fhi-berlin.mpg.de (T. Ressler).

0926-860X/$ – see front matter © 2003 Elsevier B.V. All rights reserved.
doi:10.1016/j.apcata.2003.09.013

1.1. Reaction mechanism for methanol–steam reforming and formation of CO

Suggestions in the literature on the reaction mechanisms of methanol–steam reforming can, with respect to the formation of CO, be divided into three groups: (i) CO is produced directly through the decomposition of methanol and reacts further through the water gas-shift reaction [12,13], (ii) CO is produced as a secondary product in the reverse WGS reaction [14,11], and (iii) CO formation is not considered in the reaction network [15]. In this work we studied the formal kinetic of methanol–steam reforming over a commercial $CuO/ZnO/Al_2O_3$ catalyst by use of differential and integral reaction data. Our work is particularly focused on studying the reaction scheme of CO formation and revealing a solution to decrease CO levels in the product. As reported in the literature CO levels can be influenced by the temperature of the reactor, degree of conversion of the methanol, molar ratio of methanol and water, and addition of oxygen to the methanol–steam mixture [11].

2. Experimental

Measurements of the methanol–steam reforming reaction were performed at atmospheric pressure in a tubular stainless steel reactor (10 mm i.d.). A commercial $CuO/ZnO/Al_2O_3$ catalyst from Süd-Chemie (approximately 50 wt.% Cu) [16] was used in all experiments. The reactor was placed in an aluminium heating block for better heat transfer, with six cartridge heaters of 125 W each inside the aluminium block. The temperature of the reactor was regulated by PID control of the cartridge heaters. Two thermocouples of type J (Fe versus (Cu + 43%Ni)) were used, one was placed in the aluminium block, the other one was placed in the catalyst bed. The catalyst was supported by a stainless steel fixed fine mesh grid. For flow conditioning, inert Pyrex beads of the catalyst's size (0.85–1.0 mm) were placed on top and below the catalyst bed. For steam reforming measurements the catalyst powder was first diluted with five times its weight of boron nitride (BN) and then the mixture was pressed using a cylinder stamp with a diameter of 29 mm. One gram of the mixture was put into the cylinder stamp and was pressed at 200 bar for 4 min, the pressing was repeated three times for each tablet. The tablet was then crushed into smaller particles that were sieved to obtain a defined particle size. The reactants, water, and methanol (for HPLC, purity = 99.8% (GC)) were introduced into the reactor in a molar ratio of 1 and at a liquid flow rate of 0.05–0.5 ml min^{-1} by means of an HPLC pump. Prior to the activity measurements, the catalyst was activated at 250 °C in the reaction mixture.

Product analysis begins with the separation of water and methanol from the rest of the product stream. The separation is accomplished by passing the exhaust gases through a series of cold traps, non-condensed product gases (CO, CO_2, and H_2) were separated from the unreacted water and methanol. The dry effluent gases were analyzed using a 25 m × 0.53 mm CarboPLOT P7 column in a Varian GC 3800 equipped with a thermal conductivity detector. Helium was used as carrier gas. The composition of the condensed mixture was analyzed by a second gas chromatograph Intersmat IGC 120 ml using a 50 m × 0.53 mm fused Silica PLOT CP-Wax 58 (FFAP). For the determination of the gas composition in the product, we used the calibrated gas von Messer Griesheim with the following composition (in vol.%): CO 0.5, CO_2 25, H_2 70, the rest N_2 4.5. The peak area in the chromatogram of the 0.5% volume of CO calculated by the GC is 520 U. The smallest peak area that can be still counted reproducibly by the computer is about 10 U. This indicates that the detection limit of the CO concentration is about 0.01% volume which equals to the partial pressure of CO of 5×10^{-5} kPa. Because Helium is used as carrier gas, the concentration of N_2, CO and CO_2 can be determined accurately. By means of the mass balance calculation of the dry gas the concentration of H_2 is determined. In the work of Choi and Stenger [18], they studied the methanol decomposition reaction catalyzed by a commercial $Cu/ZnO/Al_2O_3$ in the absence and presence of water (steam reforming reaction). Their results show clearly that the by products such as methane, methyl formate and dimethyl ether are significantly detected in the reaction of methanol decomposition (in the absence of water). However, no methyl formate was detected when the feed contains 43 mol% water or greater. There was no dimethyl ether formation when the feed had more than 24 mol% water and no methane was detected after a feed of 8.6 mol% of water. Since we are working on the reaction conditions where water content in feed is 50 mol% which is much greater than that used in the work of Choi and Stenger. The detection of the by-products under the reaction conditions applied in our experiments is therefore not necessary.

3. Results and discussion

3.1. Activity and stability of the $CuO/ZnO/Al_2O_3$ catalyst

Conversion of methanol at 250 °C as a function of the W/F_m ratio (W: mass of the catalyst (kg), F_m: flow rate of methanol (mmol s^{-1})) for the catalyst used in this study is depicted in Fig. 1. For these measurements 200 mg of catalyst were used and the W/F_m ratio was varied by changing the flow velocity of the methanol–water mixture between 0.05 and 0.5 ml min^{-1}. The catalyst used in this work was also used in the work of Muhler and co workers [16] in which details of its composition are given. To compare the activity of this catalyst with a similar catalyst which has been reported in the literature (Süd-Chemie, G-66 MR (52 wt.% Cu [11])) the methanol conversion versus W/F_m curve for the G-66 MR catalyst at 260 °C has also been plotted in Fig. 1. These results show little difference in methanol conversion

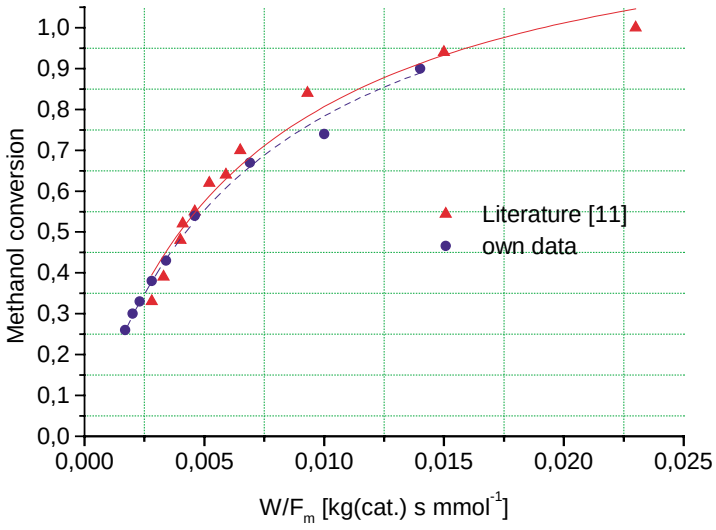

Fig. 1. Methanol conversion as a function of W/F_m ratio for two catalysts: circle, catalyst studied in this work ($T = 250\,^{\circ}C$, $H_2O/CH_3OH = 1.0$); triangle, catalyst studied in the work of Agrell et al. [11] ($T = 260\,^{\circ}C$, $H_2O/CH_3OH = 1.3$).

as a function of W/F_m ratio between the two catalysts, and the catalyst studied in this work can be considered comparable to an industrial catalyst with 52 wt.% Cu.

Typical runs of methanol conversion as a function of the W/F_m ratio for the $CuO/ZnO/Al_2O_3$ catalyst at reaction temperatures ranging from 230 to 300 °C are presented in Fig. 2. The results show that methanol conversion increased rapidly for short contact times (0–0.005 kg(cat) s^{-1} $mmol^{-1}$) at all temperatures, and that the rate of the methanol conversion as function of contact time always increased with an increasing reaction temperature. Similar results have been reported in the work of Idem and Bakhshi [17] over a different temperature range from 170 to 250 °C. They found a dramatic change in the slope of the methanol conversion versus W/F_m ratio curves between the reaction temperatures of 190 and 200 °C. Based on these results they have suggested that there are two kinetic regimes (low temperature regime $T = 190\,^{\circ}C$, high temperature regime $T = 200\,^{\circ}C$) indicating that the rate determining step for the SR reaction mechanism is different for these two temperature regimes. The experimental results that Idem reported as being in the high temperature regime are comparable to those plotted in Fig. 2 and we conclude that the conditions under which we have studied the SR reaction are all within the high temperature regime. The catalyst's stability over 320 h on stream is presented in Fig. 3. In the period from 0 to 100 h the conversion decreased slightly. There is little change in methanol conversion at times on stream between 100 and 320 h. This result agrees well with that reported in the literature [18] where the deactivation of the catalyst was measured with and without water added to methanol. It was found that in the presence of water (50%) and at 250 °C deactivation is less evident

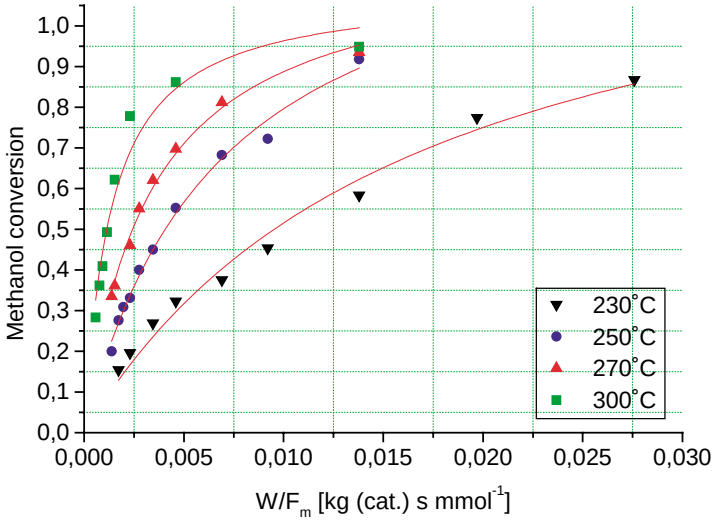

Fig. 2. Methanol conversion as a function of W/F_m ratio at different temperatures (mass of the catalyst 200 mg).

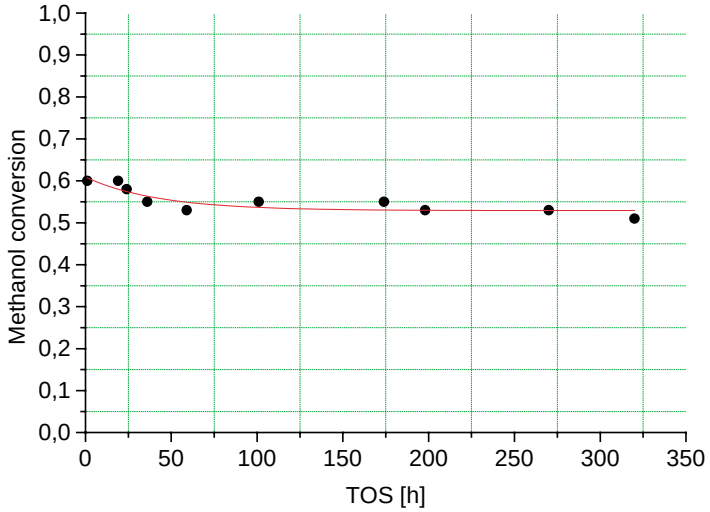

Fig. 3. Methanol conversion as a function of time on stream at 250 °C (mass of the catalyst 200 mg, W/F_m ratio 0.007 (kg(cat) s mmol^{-1})).

within the first 100 h on stream than with methanol alone. All measurements in this work were carried out within 100 h of the time of reduction in order to limit errors caused by catalyst deactivation.

3.2. Kinetic model

The reaction schemes for methanol–steam reforming considered in this work are: (i) methanol–steam reforming (SR) reaction and (ii) the reverse water gas-shift (rWGS) reaction.

$$CH_3OH + H_2O \underset{k_{-1}}{\overset{k_1}{\rightleftarrows}} 3H_2 + CO_2 \quad (1)$$

$$CO_2 + H_2 \underset{k_{-2}}{\overset{k_2}{\rightleftarrows}} CO + H_2O \quad (2)$$

For analysis of the kinetics of these reactions the power law was used as a model to fit the experimental data. Since both of the reactions are reversible processes, the equilibrium constant K can be defined as the ratio of the forward and backward reaction constants:

$$K_{SR} = \frac{k_1}{k_{-1}} = \frac{P_{H_2}^3 P_{CO_2}}{P_{CH_3OH} P_{H_2O}} \quad (3)$$

$$K_{rWGS} = \frac{k_2}{k_{-2}} = \frac{P_{CO} P_{H_2O}}{P_{CO_2} P_{H_2}} \quad (4)$$

where P is the partial pressure and k the rate constant for forward (+) and reverse (−) reactions. The rate equations for the SR reaction and reverse WGS reaction can be described as follows:

$$r_{SR} = k_1 P_{CH_3OH}^m P_{H_2O}^n - k_{-1} P_{H_2}^r P_{CO_2}^s \quad (5)$$

$$r_{rWGS} = k_2 P_{CO_2} P_{H_2} - k_{-2} P_{H_2O} P_{CO} \quad (6)$$

It is clear from the low concentrations of CO formed that the rate constant for the reverse WGS reaction is very small with respect to the SR reaction. Therefore, it was necessary to assume the reaction order of the reactants and the products for the reverse WGS reaction and we have set them to 1, as in Eq. (6). By inserting the reaction equilibrium constants K_{SR}, K_{rWGS} into Eqs. (5) and (6), the reaction rates can be written as:

$$r_{SR} = k_1 P_{CH_3OH}^m P_{H_2O}^n \left(1 - \frac{1}{K_{SR}} \frac{P_{H_2}^r P_{CO_2}^s}{P_{CH_3OH}^m P_{H_2O}^n}\right) \quad (7)$$

$$r_{rWGS} = k_2 P_{CO_2} P_{H_2} \left(1 - \frac{1}{K_{rWGS}} \frac{P_{H_2O} P_{CO}}{P_{CO_2} P_{H_2}}\right) \quad (8)$$

The equilibrium constant being a function of temperature can be calculated by means of the following thermodynamic descriptions:

$$\Delta G_{298}^0 = \Delta H_{298}^0 - T \Delta S_{298}^0 \quad (9)$$

$$\Delta G_{298}^0 = -RT \ln K_{298} \quad (10)$$

The reaction enthalpies ΔH_{298}^0 for SR reaction and reverse WGS reaction are +49 and +41 kJ mol^{-1}, the reaction entropies are +177 and +42 J mol^{-1}, and the free enthalpies ΔG_{298}^0 are −3.8 and +28.6 kJ mol^{-1}, all respectively [19]. The equilibrium constant as a function of temperature is given by the van't Hoff expression:

$$\ln K = \ln K_{298} - \frac{\Delta H_{298}^0}{R} \left\{\frac{1}{T} - \frac{1}{T_{298}}\right\} \quad (11)$$

The results of calculation of K_{SR}, K_{rWGS}, and the reciprocals of the constants at different temperatures are listed in Table 1. Because of the very small value of the reciprocal of K_{SR}, Eq. (7) can be simplified as follows:

$$r_{SR} = k_1 P_{CH_3OH}^m P_{H_2O}^n \quad (12)$$

Eqs. (8) and (12) were then used to fit the experimental reaction rate data.

Table 1
Equilibrium constants of SR reaction and reverse WGS reaction as a function of temperature

T (°C)	SR		rWGS	
	K_1 (bar^2)	K_1^{-1} (bar^{-2})	K_2	K_2^{-1}
230	1.5×10^4	6.6×10^{-5}	0.9×10^{-2}	116
250	2.4×10^4	4.2×10^{-5}	1.3×10^{-2}	80
270	3.6×10^4	2.8×10^{-5}	1.8×10^{-2}	56
300	6.4×10^4	1.6×10^{-5}	2.9×10^{-2}	35

In order to determine the reaction parameters (reaction order, reaction rate constants, and activation energies) two experimental methods were employed. First, the differential method was used in order to determine the reaction order of methanol, and then the integral method was used to determine the total reaction order and the rate constants for the SR reaction. For the differential method determination the conversion of methanol was less than 10%, the partial pressure of water was held constant, nitrogen was used as a third component, and the reaction temperature was 250 °C. Prior to measurement, the catalyst was activated in the methanol–water feed (molar ratio of 1) at 250 °C for 1 h. Through variation of the methanol partial pressure at constant water partial pressure reaction rates with the units (mol (CH_3OH) s^{-1} $g_{catalyst}^{-1}$) were determined. A log–log plot of methanol partial pressure and reaction rate is displayed in Fig. 4. Linear regression of the experimental data gave a reaction order for methanol of 0.6 ± 0.1. The catalysis experiments used to obtain this value were performed using catalyst with particle sizes between 0.71 and 1.0 mm. We have determined that under these conditions there was a significant intraparticle diffusion limitation. The reaction order observed here is thus an apparent reaction order. For large values of the Thiele modulus (ratio of the surface reaction rate to the diffusion rate), i.e. for a system with significant diffusion limitation, the apparent reaction order n_{app} is related to the true reaction order n_t by [20]

$$n_{app} = \frac{n_t + 1}{2} \quad (13)$$

The true reaction order of methanol obtained using Eq. (13) is 0.2. This value is comparable to that reported in the literature [21] of 0.26, obtained in a study of the kinetics of steam reforming of methanol over a BASF S3-85 $CuO/ZnO/Al_2O_3$ catalyst. The absence of a diffusion limitation was determined in the study of the BASF catalyst by a three-fold variation in the catalyst particle size (0.15–0.59 mm).

We then determined the total reaction order and the rate constants for the SR reaction by the integral method as follows. A wide range of methanol and water conversions as a function of contact time were measured for temperatures from 230 to 300 °C and these data are presented in Figs. 5–8.

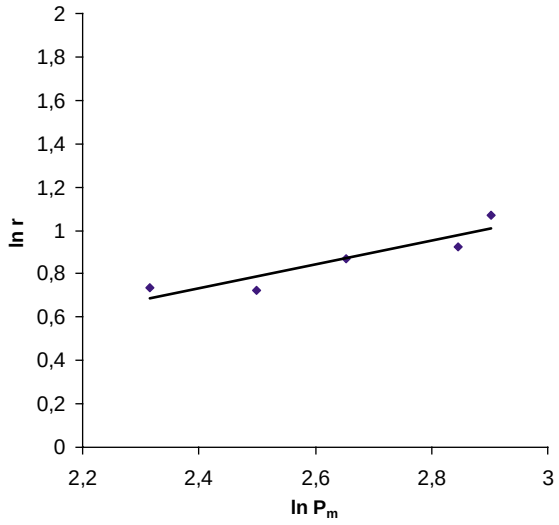

Fig. 4. Reaction rate of methanol–steam reforming as a function of methanol partial pressure at constant water partial pressure at 250 °C (mass of the catalyst 40 mg, W/F_m ratio 0.33–0.15 (kg(cat) s mmol^{-1})).

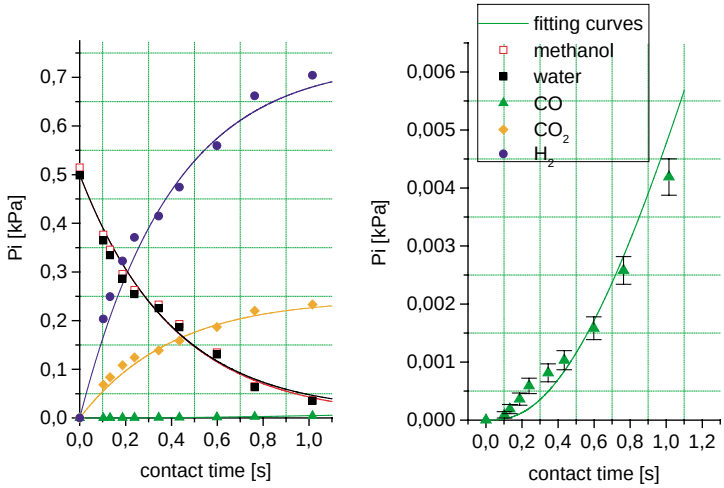

Fig. 5. Partial pressures of components of the product stream as a function of contact time at 230 °C, experimental data and fitting results.

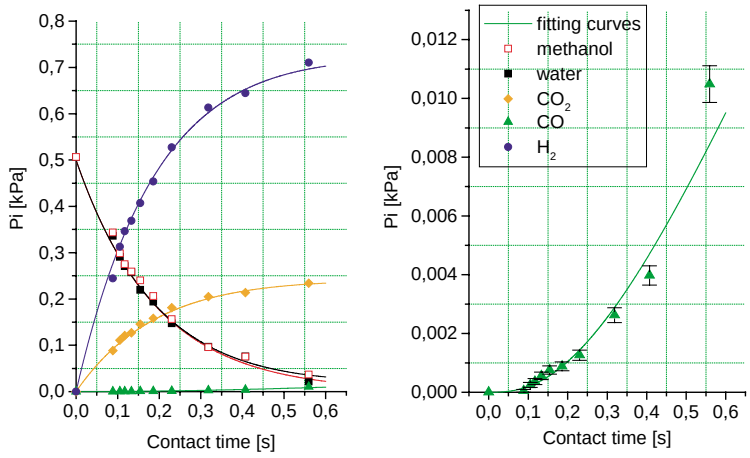

Fig. 6. Partial pressures of components of the product stream as a function of contact time at 250 °C, experimental data and fitting curves.

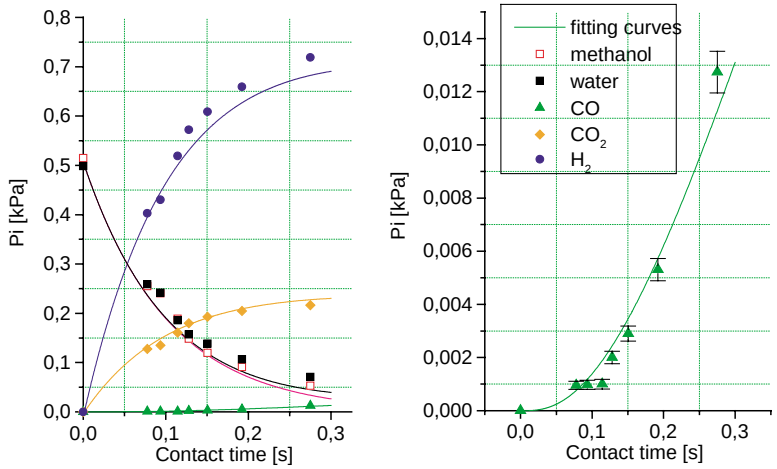

Fig. 7. Partial pressures of components of the product stream as a function of contact time at 270 °C, experimental data and fitting curves.

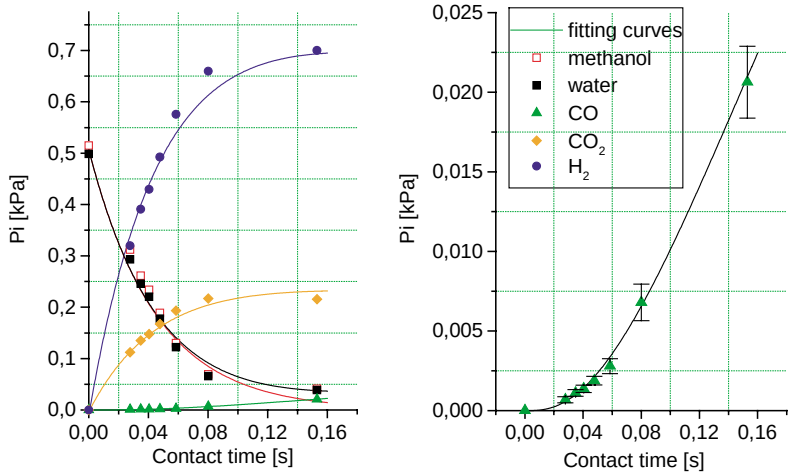

Fig. 8. Partial pressures of components of the product stream as a function of contact time at 300 °C, experimental data and fitting curves.

Eqs. (8) and (12) were used to fit the experimental data for all temperature ranges. Due to the change in the number of moles in the gas as the methanol–steam reforming reaction proceeds, (2 mol reactant, 4 mol product), the contact time was defined with the following equation:

$$\tau = \frac{V_{\text{catalyst}}}{\dot{V}_{\text{gas}}(1+\alpha X)} \quad (14)$$

where V_{catalyst} is the volume of the catalyst bed in the reactor, $\dot{V}_{\text{gas}}$ the volume of gaseous methanol and water, α the relative change of the gas volume in the reactor if the conversion is complete, and X the fractional conversion of methanol. Determination of the reaction order and rate constants was accomplished by fitting the simulation to the measured data with variation of the total reaction order and the rate constants until a good agreement is obtained. Specifically a total reaction order was chosen, and the fit was optimized by variation of the reaction rate constants. A Runge–Kutta method was used to solve the differential equations for the SR and rWGS reactions, and the experimental data was fit by means of a simplex least-square method. A new total reaction order was then selected and the data was again fit by variation of the rate constants. This procedure was repeated until an optimal fit was achieved. By this method a total reaction order for methanol and water ($m + n$ in Eq. (12)) of 1 was determined to fit the data well.

The reaction products were hydrogen, carbon dioxide, and a very small concentration of carbon monoxide. For all reaction temperatures measured there was no significant change in the molar ratio of methanol and water with increasing contact time. The partial pressure of hydrogen and carbon dioxide increased with increasing contact time. As expected from the SR reaction scheme, Eq. (1), the ratio of the partial pressures of hydrogen and carbon dioxide was about 3 at all reaction temperatures and levels of conversion. Thus, the scheme of the SR reaction as expressed by Eq. (12) describes well the methanol–steam reforming reaction with a $CuO/ZnO/Al_2O_3$ catalyst. The small amount of CO produced increases with increasing contact time and can be described by the reaction model (i.e. Eqs. (8) and (12)). This indicates that CO is a consecutive product formed by the reverse WGS reaction from the products of the SR reaction, H_2 and CO_2. It is clear from Fig. 5 that, although the formation of CO can be described satisfactorily with the reverse WGS reaction, the "real" reaction kinetics are more complex. Specifically, there seems to be a change in the controlling kinetic of CO formation for conversions > 70%. This is clearly visible in the change in CO concentration with increasing contact time shown in Fig. 5. At contact times less than 0.5 s there is more CO present than is predicted by the simulation. At higher contact times there is a distinct change in the rate of CO formation. A similar change in kinetic is discernable in Fig. 6, also at about 70% conversion, or at a contact time of 0.15 s for the reaction at 250 °C. As conversion increases the changing gas phase may induce changes in the active surface. Alternatively, the change in rate law may indicate blocking of particular sites on the heterogeneous surface of the copper particles. A strained copper bulk [22], for instance, may result in heterogeneity in the sites active for CO formation with specific sites exhibiting a higher sticking coefficient for CO than unstrained copper metal (0.87, Cu(1 1 1)). The CO level as a function of contact time will be discussed later in more detail.

The results in Figs. 5–8 show that by using the reaction schemes in Eqs. (8) and (12) the simulation agrees well with the experimental data. In addition, we did not observe any inhibition effects due high concentrations of CO_2 and H_2 produced in the SR process at high conversions. Such an effect would be expressed in the data as a decrease in the rate of reaction at higher conversion in comparison to the simulation which does not account for an inhibition effect. We did not observed such deviations indicative of product inhibitions. The reaction rate constants for the steam reforming reaction, k_1, and the reverse water gas-shift reaction, k_2, were the free parameters used in the simulation to fit the experimental data. Log(k) as a function of reciprocal temperature is presented in Fig. 9. The apparent activation energy and pre-exponential factor for the steam reforming reaction obtained by linear regression are:

$$E_a = 76\,\text{kJ mol}^{-1}$$

$$k_0 = 8.8 \times 10^8 (\text{s}^{-1}\,\text{g}_{\text{cat}}^{-1})$$

Similarly, using data presented in Fig. 9, E_a and k_0 were determined for the reverse WGS, and WGS reactions.

(i) Reverse WGS: $E_a = 108\,\text{kJ mol}^{-1}$, $k_0 = 6.5 \times 109\,(\text{bar}^{-1}\,\text{s}^{-1}\,\text{g}_{\text{cat}}^{-1})$

(ii) WGS: $E_a = 67\,\text{kJ mol}^{-1}$, $k_0 = 4.0 \times 107 (\text{bar}^{-1}\,\text{s}^{-1}\,\text{g}_{\text{cat}}^{-1})$

All reaction parameters for SR, reverse WGS, and WGS reactions obtained in this work are summarized in Table 2. The activation energy determined in this work is an apparent activation energy corresponding to a catalyst with particle sizes of 0.71–1.0 mm in which internal diffusion limitation occurred. Therefore, the activation energy is lower in

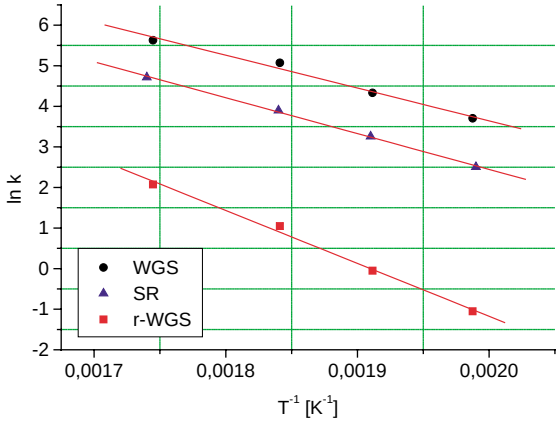

Fig. 9. Reaction rate constants for SR reaction, reverse WGS reaction, and WGS reaction as a function of reciprocal temperatures.

Table 2
Experimental results of reaction rate constants, activation energy and pre-exponential factor for SR reaction, reverse WGS reaction and calculated result of WGS reaction

	SR, k ($s^{-1}\ g_{cat}^{-1}$)	rWGS, k ($bar^{-1}\ s^{-1}\ g_{cat}^{-1}$)	WGS, k ($bar^{-1}\ s^{-1}\ g_{cat}^{-1}$)
T (°C)			
230	2.5	0.07	7.8
250	5.2	0.19	14.6
270	9.8	0.57	31.7
300	22.3	1.59	54.8
E_a (kJ mol^{-1})	76	108	67
k_0	8.8×10^8	6.5×10^9	4.0×10^7

comparison to that reported in the literature [21] which was calculated from data obtained using smaller particle sizes where mass transport limitations were absent.

3.3. CO formation

CO partial pressure as a function of contact time for all temperatures investigated is presented in Figs. 5–8. CO partial pressure increases monotonically with an increasing contact time. The contact time span for all the experiments was chosen to include a wide range of methanol conversions ranging up to almost 90%. The CO levels at all reaction temperatures (230–300 °C) are far below those predicted by equilibrium calculations based on water gas-shift reaction, and this indicates that CO_2 can not be formed from CO through the WGS reaction. This result agrees well with the literature [11,21]. The selectivity of CO and CO_2 as a function of contact time is depicted in Fig. 10. As contact time approaches 0, selectivity to CO goes to 0 showing that CO is a secondary product. These results show clearly that CO is produced in a consecutive reaction and that CO is not formed as a primary product of methanol decomposition. Consistent with this reaction scheme the selectivity to CO_2 is constant up to a contact time of 0.2 s and there after decreases slightly. By employing the reverse WGS reaction to describe the CO formation as a consecutive product, the experimental data have been simulated accurately. Conversely, reaction schemes for the methanol–steam reforming reaction on copper-based catalysts that include the decomposition of methanol to produce CO followed by the WGS reaction [23–26] were not able to fit our experimental data. Several investigations concerning the WGS reaction on commercial ($CuO/ZnO/Al_2O_3$) catalysts have been performed under reaction conditions similar to those employed in this work. Results reported in the literature [21] have shown that the WGS reaction does not take place under the condition of the SR reaction, although the $CuO/ZnO/Al_2O_3$ catalyst is known to be active for the low temperature WGS reaction. In this study high concentrations of CO were added to a reactant mixture of methanol and water, and there was no significant change in the rate of hydrogen production or in the hydrogen to CO_2 ratio, the amount of CO passing through the reactor remained unchanged. One reason suggested for this minimal participation of the WGS reaction in the presence of methanol and water vapor is competitive adsorption between methanol and CO [21]. In an infrared spectroscopy study it was found that methanol and methyl formate adsorb more strongly on a copper surface as compared to carbon monoxide [27]. The blockage of the catalyst's surface through methanol and methyl formate prevents the reaction of CO and water. Takahashi et al. [15] have reported that the WGS reaction was also blocked in the presence of methanol for a Cu/SiO_2 catalyst.

3.4. Influence of intraparticle diffusion limitation to the CO formation

The study of intraparticle diffusion limitation of two different particle sizes (0.71–1.0 and 0.45–0.5 mm), is presented in Fig. 11. Result shows that the catalyst with smaller particle size produces the higher methanol conversion. The dependence of methanol conversion on the particle size

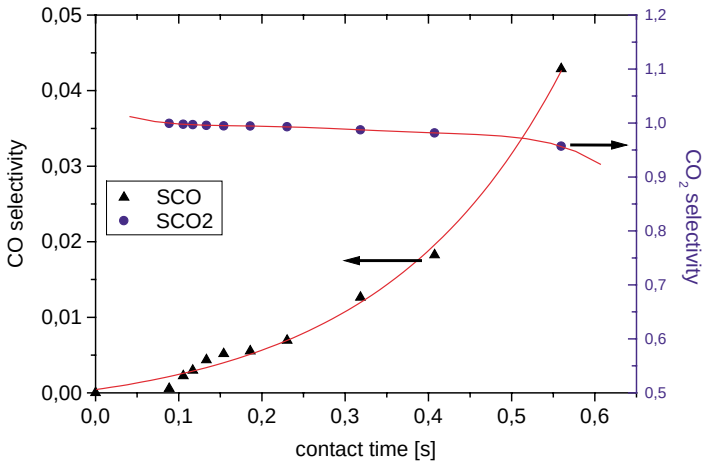

Fig. 10. CO and CO_2 selectivity as a function of contact time at 250 °C.

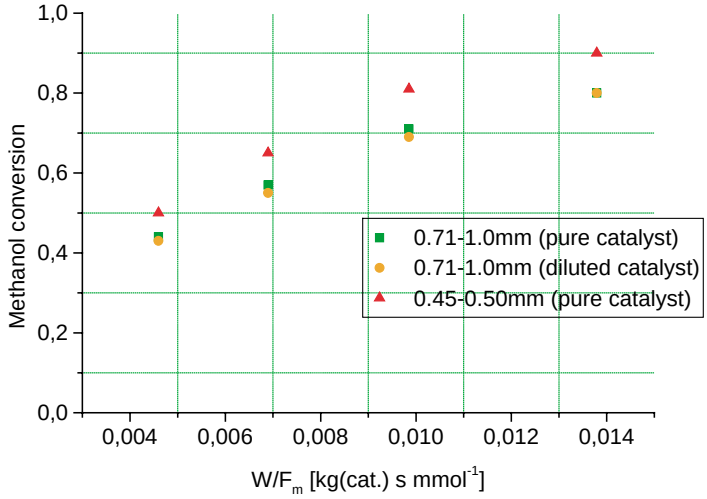

Fig. 11. Methanol conversion as a function of W/F_m ratio carried out on different catalyst particle sizes (0.45–0.5 mm (pure catalyst); 0.71–1.0 mm (pure catalyst); 0.71–1.0 mm (diluted with five-fold amount of boron nitride)).

indicates the presence of intraparticle diffusion limitation as mentioned earlier. CO concentration as a function of methanol conversion measured for catalysts with different particle sizes is plotted in Fig. 12. At the same methanol conversion, the CO level obtained from larger particles was found to be higher than that obtained from smaller particles. The increase of the CO concentration with increasing particle size and thus, increasing diffusion limitation is again consistent with the finding that CO is formed as a consecutive product in the reverse WGS reaction. This result agrees well with our results relating to the kinetics of CO formation (CO levels as a function of contact time). CO concentration as a function of methanol conversion measured on pure and five-fold diluted catalyst with the same particle sizes is depicted in Fig. 13. Evidently, the catalyst diluted with boron nitride produced much less CO than that without dilution. The difference becomes significant at methanol conversions

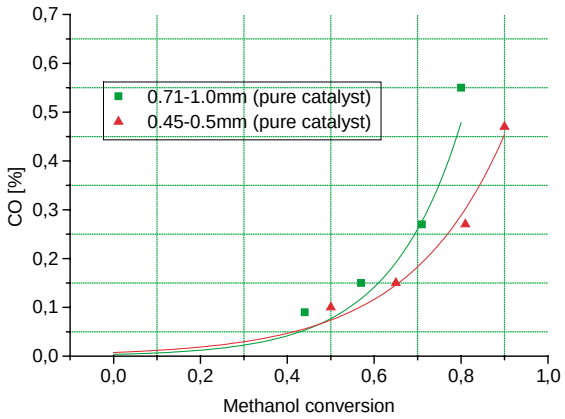

Fig. 12. CO formation during MSR as a function of methanol conversion for catalysts with different particle sizes (0.71–1.0 mm (pure catalyst), 0.45–0.5 (pure catalyst)).

higher than 0.6. The influence of diluting the catalyst with boron nitride on CO formation can be interpreted using the scheme depicted in Fig. 14. The circles with different intensities depict particles with different catalyst concentrations (dark: pure catalyst, light: diluted catalyst). Conversion in particles of the pure catalyst is much higher than that in particles of the diluted catalyst. This results in higher concentrations of hydrogen and carbon dioxide in the particle centers. The rate of the consecutive CO formation by reverse WGS reaction is a function of the hydrogen and the carbon dioxide concentrations and so more CO is produced in the pure catalyst than in the diluted catalyst. Further studies on this subject are necessary to obtain more quantitative information. Our results clearly show that the concentration of CO formed as a consecutive product is influenced by the particle size of the catalyst which relates to the intraparticle diffusion limitation and the treatment of the catalyst, e.g. catalyst dilution with inert material. It has previously been reported that the level of CO produced in methanol–steam reforming over copper-based catalysts can be influenced by the following factors:

(i) Reaction temperature [11,28].
(ii) Contact time, conversion of methanol, respectively [11].
(iii) Molar ratio of methanol and water [11,18].
(iv) Introducing oxygen to methanol–steam mixture [11].

Based on this work it becomes clear that additional factors influence the formation of CO:

(v) Particle size of the catalyst (intraparticle diffusion limitation).
(vi) Mechanical treatment of the catalyst, i.e. dilution.
(vii) Heterogeneity of the copper surface resulting from defects in the Cu bulk or different morphology of the copper particles.

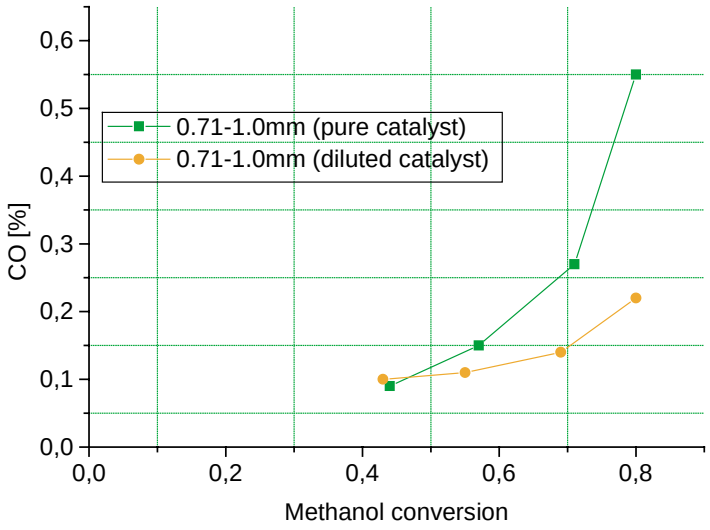

Fig. 13. CO formation as function of methanol conversion for catalysts diluted and not diluted.

With respect to the intraparticle diffusion limitation that influences the amount of CO formed, the objective is to minimize the diffusion path. For packed bed reactors lower levels of CO can be achieved by using a very small particle size, where intraparticle diffusion limitation is absent. In such a reactor the grain size of the catalyst in the reactor plays an important role for the flow behavior. In order to achieve plug flow behavior of the gas through the catalyst bed, the diameter of the catalyst in general should be smaller than 0.1 times the inner diameter of the reactor. However, use of excessively small particles of catalyst in a reactor can increase the pressure drop across the reactor. In order to exclude intraparticle diffusion limitations and to keep a certain particle size which obeys the plug flow criterion and produces minimal pressure drop, an egg-shell catalyst with the active component coated on the surface of a support material can

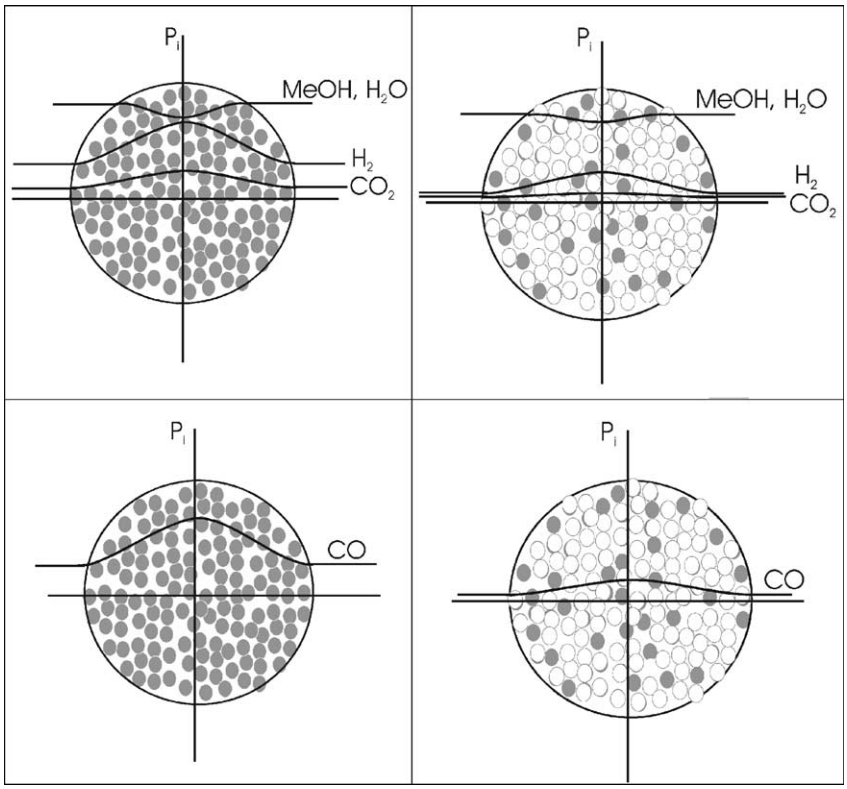

Fig. 14. Description of the partial pressure profile of the components (reactants, products) as a function of particle radii for catalysts diluted and not diluted.

be used. Using an egg-shell catalyst for methanol–steam reforming over Cu catalysts may be potentially advantageous, however, the ability to synthesize such a catalyst, in light of the complexity of the synthesis of Cu catalysts, would require investigation. Alternatively, minimal levels of CO, and particle size that obeys the plug flow criterion with less pressure drop may be achieved by diluting the catalyst with inert material. Treatment of the catalyst by dilution is a simple step which significantly influence the CO levels and will provide no substantial disadvantages to the process. Similarly, for on-board SR production of H_2, coating the walls of a micro-tube reactor with layers of catalysts sufficiently thin to exclude diffusion limitations may be feasible. Even simpler in design, if not implementation, would be to make the tubes themselves out of Cu or a Cu containing composite material which may be activatable by suitable oxidation and reduction treatments. These proposed chemical engineering solutions should be considered for implementation of the production of H_2 for fuel cells through the steam reforming of methanol. Additionally, the complex kinetics of the formation of CO, that deviate from the simplified reaction mechanism assumed here and highlights the complexity of the active surface, indicate that in addition to the engineering solutions proposed, there is room for improvement in the catalyst itself. The defect type and density in the bulk and at the surface of the copper metal and, hence, catalytic properties may be substantially improved by appropriate preparation and treatment procedures of improved copper catalysts.

4. Conclusions

A kinetic study of methanol–steam reforming over commercial catalyst $CuO/ZnO/Al_2O_3$ has been performed at atmospheric pressure over a wide temperature range (230–300 °C). The reaction scheme used is the direct formation of CO_2 and hydrogen by the SR reaction and the formation of CO as a consecutive product by the reverse WGS reaction. The power rate law and the kinetic reaction parameters of the SR reaction and the reverse WGS reaction were used to fit the experiment data resulting in the following:

$$r_{SR} = k_1 P_{CH_3OH}^{m} P_{H_2O}^{n} \quad m = 0.6;\ n = 0.4$$

$$\text{apparent } E_a = 76\,\text{kJ mol}^{-1}, \qquad k_0 = 8.8 \times 108\,(\text{s}^{-1}\,\text{g}_{cat}^{-1})$$

$$r_{RWGS} = k_2 P_{CO_2} P_{H_2} - k_{-2} P_{H_2O} P_{CO}$$

$$\text{apparent } E_a = 108\,\text{kJ mol}^{-1},$$

$$k_0 = 6.5 \times 109\,(\text{bar}^{-1}\,\text{s}^{-1}\,\text{g}_{cat}^{-1})$$

Internal diffusion limitations were present for the particle size of catalyst used in this study and so only apparent activation energies for this particle size can be reported. A simulation employing the SR reaction and the reverse WGS reaction to describe the methanol–steam reforming process over a $CuO/ZnO/Al_2O_3$ catalyst fit the kinetic data measured at 230–300 °C well. The monotonic increase of CO partial pressure as a function of contact time as well as the limit of no selectivity for CO as the contact time approaches 0, shows that CO is formed as a consecutive product. Although the majority of CO is produced as a secondary product, the deviation from a single rate law, over the broad range of conversions investigated, indicates that the complexity of the reaction kinetics, particularly at lower temperatures, is greater than described by the model given here.

In addition to the parameters that have already been reported in the literature as influencing the production of CO (reaction temperature, contact time, molar ratio of methanol and water, and addition of oxygen to the methanol–steam feed), the CO concentration can also be influenced by the particle size of the catalyst through its effect on intraparticle diffusion limitation. The greater the mass transport limitation in the catalyst particle the higher the concentration of CO in the product stream. Suppressing the CO levels by using very small particles of pure catalyst in which internal diffusion limitations are negligible can reduce CO formation, but this solution may not be desirable due to an increased pressure drop in the reactor. Potential solutions that can be applied to reduce the CO concentration are (i) the use of egg-shell catalyst; however, this kind of catalyst is in general employed for noble metals and the synthesis route is complex, (ii) the use of a microtube reactor with either tube walls thinly coated with catalyst, or with Cu tubes which may be activatable, (iii) use of a diluted catalyst, or (iv) improve surface and bulk defect type and density by appropriate preparation and treatment procedures. Further study is needed to quantify our ability to suppress CO formation through these solutions.

Acknowledgements

The authors gratefully acknowledge financial support from the ZEIT foundation (project "*Nanochemistry for the automobiles of the future*", http://www.ZEIT-Stiftung.de).

References

[1] B. Lindström, L.J. Pettersson, Int J. Hydrogen Energy 26 (2001) 923.
[2] K. Narusawa, M. Hayashida, Y. Kamiya, H. Roppongi, D. Kurashima, K. Wakabayashi, JSAE Rev. 24 (2003) 41.
[3] O. Korotkikh, R. Farrauto, Catal. Today 62 (2000) 249.
[4] C.D. Dudfield, R. Chen, P.D. Adcock, Int J. Hydrogen Energy 26 (2001) 763.
[5] H. Oh, R.M. Sinkevitch, J. Catal. 142 (1993) 254.
[6] J. Han, I.S. Kim, K.S. Choi, J. Power Sources 86 (2000) 223.
[7] Y.M. Lin, G.L. Lee, M.H. Rei, Catal. Today 44 (1998) 343.
[8] N. Itoh, Y. Kaneko, A. Igarashi, Ind. Eng. Chem. Res. 41 (2002) 4702.
[9] J. Han, I.S. Kim, K.S. Choi, Int J. Hydrogen Energy 27 (2002) 1043.
[10] I.S. Wieland, I.T. Melin, I.A. Lamm, Chem. Eng. Sci. 57 (2002) 1571.

[11] J. Agrell, H. Birgersson, M. Boutonnet, J. Power Sources 106 (2002) 249.
[12] R. Peters, H.G. Düsterwald, B. Höhlein, J. Power Sources 86 (2000) 507.
[13] B.A. Peppley, J.C. Amphlett, L.M. Kearns, R.F. Mann, Appl. Catal. 179 (1999) 21.
[14] J.P. Breen, J.R.H. Ross, Catal. Today 51 (1999) 521.
[15] K. Takahashi, N. Takezawa, H. Kobayashi, Appl. Catal. 2 (1982) 363.
[16] T. Genger, O. Hinrichsen, M. Muhler, Catal. Lett. 59 (1999) 137.
[17] R.O. Idem, N.A. Bakhshi, Chem. Eng. Sci. 51 (1996) 3697.
[18] Y. Choi, H.G. Stenger, Appl. Catal. B 38 (2002) 259.
[19] P.W. Atkins, Physikalishe Chemie, VCH, Weinheim, 1987, p. 859.
[20] H.S. Fogler, Elements of Chemical Reaction Engineering, 3rd edition, Prentice Hall PTR (1998) 754.
[21] C.J. Jiang, D.L. Trimm, M.S. Wainwright, Appl. Catal. 93 (1993) 245.
[22] M. M Günter, T. Ressler, B. Bems, C. Büscher, T. Genger, O. Hinrichsen, M. Muhler, R. Schlögl, Catal. Lett. 71 (2001) 37.
[23] V. Pour, J. Barton, A. Benda, Coll. Czech. Chem. Commun. 40 (1975) 2923.
[24] J. Barton, V. Pour, Coll. Czech. Chem. Commun. 45 (1980) 3402.
[25] E. Santacesaria, S. Carra, Appl. Catal. 5 (1983) 345.
[26] J.C. Amphlett, M.J. Evans, R.F. Mann, R.D. Weir, Can. J. Chem. Eng. 63 (1985) 605.
[27] D.M. Monti, W. Cant, D.L. Trimm, M.S. Wainwright, J. Catal. 100 (1986) 17.
[28] B. Lindström, L.J. Petterson, P.G. Menon, Appl. Catal. A 234 (2002) 111.